

Research Articles | Systems/Circuits

Fast-spike interneurons in visual cortical layer 5: Heterogeneous response properties are related to thalamocortical connectivity

<https://doi.org/10.1523/JNEUROSCI.1116-24.2024>

Received: 12 June 2024

Revised: 1 November 2024

Accepted: 26 November 2024

Copyright © 2024 the authors

This Early Release article has been peer reviewed and accepted, but has not been through the composition and copyediting processes. The final version may differ slightly in style or formatting and will contain links to any extended data.

Alerts: Sign up at www.jneurosci.org/alerts to receive customized email alerts when the fully formatted version of this article is published.

1 **Fast-spike interneurons in visual cortical layer 5: Heterogeneous response**
2 **properties are related to thalamocortical connectivity**

3
4 Chuyi Su¹, Rosangela F Mendes-Platt¹, Jose-Manuel Alonso^{1,2}, Harvey A Swadlow^{1,2},
5 Yulia Bereshpolova¹

6 ¹Dept. of Psychological Sciences University of Connecticut, Storrs CT; ²Dept. Biological
7 Sciences, SUNY-Optometry, New York, NY

8 Correspondence should be addressed to Yulia Bereshpolova at

9 yuliya.bereshpolova@uconn.edu

10 **Abstract (250 words maximum, including citations, 250 words now)**

11 Layer 4 of rabbit V1 contains fast-spiking GABAergic interneurons (suspected inhibitory
12 interneurons, SINs) that receive potent synaptic input from the LGN and generate fast,
13 local feed-forward inhibition. These cells display receptive fields with overlapping
14 ON/OFF subregions, non-linear spatial summation, very broad orientation/directional
15 tuning, and high spontaneous and visually-driven firing rates. Such fast-spike
16 interneurons are also found in layer 5 (L5), which receives a much sparser input from
17 the LGN, but the response properties and thalamocortical connectivity of L5 SINs are
18 relatively unstudied. Here, we study L5 SINs in awake rabbits (both sexes) and
19 compare their response properties with previously studied SINs of L4. We also assess
20 thalamocortical connectivity of L5 SINs, examining both cross-correlation of
21 retinotopically aligned LGN-SIN spike-trains and L5 SIN responses to electrical
22 stimulation of the LGN. These analyses confirmed that many L5 SINs, like L4 SINs,
23 receive a strong and fast monosynaptic drive from the LGN. Moreover, these LGN-
24 connected L5 SINs had response properties that were similar to those of L4 SINs and
25 were predominantly found in the upper half of L5. By contrast, L5 SINs with longer
26 synaptic latencies to LGN stimulation displayed (1) sharper orientation tuning, (2) longer
27 visual response latencies, (3) lower spontaneous and (4) visually-driven firing rates, and
28 (5) were found in the deeper half of L5. We suggest that the long-latency synaptic
29 responses in such L5 SINs reflects a multi-synaptic intracortical pathway that generates
30 a different constellation of response properties than seen in L5 SINs that are driven
31 directly by LGN input.

32
33 **Significance Statement (96 words):**

34 Fast-spike GABAergic interneurons are found across the entire depth of the visual
35 cortex but may have very different response properties and functions in each cortical

36 layer depending on a host of factors that are specific to the different layers. In layer 4,
37 they are known to receive potent synaptic input from the thalamus and generate fast,
38 local feed-forward inhibition. In layer 5, they are thought to receive less direct thalamic
39 input and be strongly dominated by intracortical input. Here, we show that some layer-5
40 interneurons receive powerful monosynaptic input from LGN and have visual response
41 properties more similar to layer 4 interneurons than those receiving little direct LGN
42 input.

43

44 **Introduction (650 words limit, 531 words)**

45 Fast spike GABAergic interneurons are found in layers 2-6 of sensory neocortex.
46 However, studies of their sensory response properties and thalamocortical connectivity
47 have been largely limited to layer 4 (L4) (Swadlow and Gusev, 2001; Gabernet et al.,
48 2005; Stoelzel et al., 2008; Zhuang et al., 2013; Bereshpolova et al., 2020; Liew et al.,
49 2021). In L4 of rabbit visual cortex (V1), putative fast spike GABAergic interneurons
50 (suspected inhibitory interneurons, SINs) display “complex” receptive fields (RFs), with
51 highly overlapped ON and OFF sub-regions, very broad (or no) orientation tuning, and
52 nonlinear spatial summation to drifting visual stimuli (F1/F0 ratios of < 1). In addition, L4
53 SINs in rabbit V1 receive a highly convergent input from the retinotopically aligned
54 region of the lateral geniculate nucleus (LGN). Similarly, SINs of both rodent and rabbit
55 somatosensory barrel cortex (S1) receive strong convergent inputs from somatotopically
56 aligned regions of ventrobasal thalamus (Swadlow, 2003; Bruno and Simons, 2002).
57 These strong thalamocortical inputs to sensory cortical L4 SINs are thought to mediate
58 a rapid and potent feedforward inhibition onto local spiny cells that shapes both
59 temporal and spatial response properties (Ferster and Miller, 2000; Sun et al., 2006;
60 Cruikshank et al., 2007).

61 L5 of sensory neocortex also contains a significant population of fast-spike
62 GABAergic interneurons, but the density of thalamocortical inputs to L5 is relatively low
63 when compared to L4, both in V1 and S1 (Stoelzel et al., 2008; El-Boustani et al., 2020;
64 Ji et al., 2016; Zhuang et al., 2021). However, L5 does receive a rich input from
65 superficial cortical layers and, according to the “canonical” circuitry of Gilbert and Wiesel
66 (1983), the inputs from superficial layers dominate the visual responses of L5 neurons
67 (Petreanu et al., 2007; Zarrinpar and Callaway, 2016; Quiquempoix et al., 2018; but see
68 Constantinople and Bruno, 2013). Given such differences between L4 and L5 in
69 thalamocortical and intracortical circuitry, here we ask how the visual response
70 properties and thalamocortical connectivity of SINs in L5 and L4 differ. To do this, we
71 study the visual response properties of L5 SINs in rabbit V1 and compare them with the
72 properties of L4 SINs that we have previously studied using near identical methods
73 (Zhuang et al., 2013). We also assess the synaptic connectivity of L5 SINs with the LGN
74 using both cross-correlation analysis of retinotopically aligned LGN-SIN pairs, and
75 electrical stimulation of the LGN. We found that response properties of most L5 SINs
76 are remarkably similar to the properties of previously studied L4 SINs. However, there
77 was considerably more heterogeneity in the response properties of the L5 SINs, some

78 of which were related to differences among L5 SInS in thalamocortical connectivity. For
79 example, L5 SInS with longer synaptic latencies to thalamic stimulation were found
80 deeper in L5 and were more sharply tuned to stimulus orientation than those with short
81 synaptic latencies. Moreover, cross-correlation analysis showed that only L5 SInS with
82 short synaptic latencies to thalamic stimulation were monosynaptically connected to
83 retinotopically aligned LGN neurons. Thus, our results indicate fundamental similarities
84 in the response properties of L4 and L5 fast-spike GABAergic interneurons, but also
85 differences that are related to thalamocortical connectivity and depth within L5.

86

87 **Materials and Methods**

88 We recorded neurons in LGN and retinotopically aligned regions of the primary
89 visual cortex (V1) from two male and one female awake adult Dutch-Belted rabbits. All
90 experimental procedures were conducted in accordance with National Institutes of
91 Health guidelines and were approved by the University of Connecticut Animal Care and
92 Use Committee.

93

94 **Animal preparation and experimental design**

95 The general surgical procedures for chronic recordings are similar to those
96 previously published by our group (Bereshpolova et al., 2006; 2020; Zhuang et al.,
97 2013; Su et al., 2024) and are reported briefly here. Skin and fascia above the skull
98 were removed under Ketamine/Xylazine/Acepromazine (40/5/2 mg/kg) anesthesia using
99 aseptic procedures. A head-restraint stainless-steel bar was affixed to the skull with
100 acrylic cement. The exposed portions of skull were covered with medical grade silastic
101 compound to provide a buffer for the wound margins from the acrylic cement.
102 Subsequently, microelectrodes implantation was performed after two weeks of recovery.
103 A seven-channel concentric, independently moveable microelectrode system (Swadlow
104 et al., 2005a) was chronically implanted in the monocular region of V1 (Fig. 1A). Single
105 unit activities and cortical local field potentials (LFP) were obtained using 40 μm
106 diameter, quartz-insulated, platinum-tungsten electrodes tapered and sharpened to a
107 fine tip with impedance 1.5 – 3 Mohm. Multi-unit activity from superficial layers of the
108 superior colliculus (SC) was simultaneously recorded by a similar 3-channel microdrive
109 system. Three stimulation electrodes (parylene-c insulated platinum/iridium micro wire)
110 were implanted within the retinotopically aligned region of the LGN for identification of
111 fast-spike interneurons in V1 and three stimulation electrodes were implanted in the SC
112 for antidromic identification of corticotectal neurons. The experiment also involved
113 recording hippocampal EEG through three electrodes implanted above and below the
114 CA1 layer to monitor brain state. Cortical EEG was recorded using one electrode placed
115 above the somatosensory cortex for additional brain state monitoring. All
116 electrophysiological activity was acquired using a Plexon data acquisition system.

117 To investigate thalamocortical connectivity between LGN neurons and L5 SINs, a
118 7-channel microelectrode system (Swadlow et al., 2005a), akin to the one detailed
119 earlier, was implanted in the LGN for chronic recordings. A small diameter craniotomy
120 (~ 1mm) was performed over retinotopically aligned region of V1. A fine-diameter single
121 electrode was moved through the cortical depth by a Narishige manipulator to record L5
122 SINs. The spontaneous activities of both LGN neurons and the retinotopically aligned
123 L5 SINs were simultaneously recorded for subsequent cross-correlation analysis. For
124 each pair of LGN and L5 SIN, a minimum of 5000 spontaneous LGN spikes were
125 collected to assess thalamocortical connectivity, providing valuable insights into the
126 functional interactions between these neural populations.

127 **Identification of layer 5**

128 The identification of cortical layers relied on detecting the depth of the reversal of
129 stimulus-evoked LFPs in V1. These LFPs were induced by a brief (20 ms) flash of a 15–
130 20 degrees circular bright visual stimulus. Histological evidence (Stoelzel et al., 2008)
131 showed that the upper border of layer 5 was ~ 500 μm below the reversal point, and the
132 upper border of layer 6 was ~ 300 μm below the upper border of layer 5 (Stoelzel et al.,
133 2017). Therefore, layer 5 was estimated from 500 to 800 μm below the reversal point of
134 the flash-evoked potential. In addition, we identified corticotectal (CTect) neurons by
135 antidromic stimulation. Because the vast majority of CTect neurons in rabbits (as in
136 other mammals) are found in L5, if a second neuron is found very near to a CTect
137 neuron, this provides confirmatory evidence that the second neuron is also in layer 5.

138 **Identification of SINs**

139 SINs were identified by a high-frequency discharge of 3 or more spikes to the
140 thalamic stimulus, with a minimal inter-spike interval of less than 1.667 ms (600 Hz, Fig.
141 1B, Swadlow, 1989, 2003; Zhuang et al., 2013). For each cell, we electrically stimulated
142 the thalamus (rectangular voltage pulses, 0.2 ms duration, range: < 1 V – 45 V) and
143 measured the stimulus threshold, latency of the first spike, and minimum interspike
144 interval. Only SINs estimated to be in L5 (recorded within 500 to 800 μm below the
145 reversal point of the flash-evoked potential) were included in this study. SINs also have
146 short spike waveform duration, but this was not used as an identification criterion (See
147 Results & Fig. 1C).

148 **Visual stimulations and eye movement control**

149 Visual stimulation protocol was similar to those previously published (Zhuang et
150 al., 2013; Su et al., 2024). Visual stimuli were generated through a custom-made
151 program (Visual C++, DirectX 7) and displayed on a CRT monitor (NecMultiSync,
152 primary monitor, 40 x 30 cm, mean luminance: 48 cd/m², refresh rate: 160Hz). The
153 reverse correlation method (Jones and Palmer, 1987) was employed to generate maps
154 of RFs from sparse noise stimuli, consisting of light and dark squares. During testing of
155 visual response properties, the RF center was continuously monitored by dynamic
156 calculation of RF position from multi-unit recordings in the SC. Sparse noise stimulation

157 was presented on a second LCD monitor, positioned next to the main monitor. If an eye
158 movement occurred during testing, the relation between the RF center of the cortical
159 cell and the SC multiunit RF center was used to dynamically place the stimulus on the
160 cortical RF (See Su et al., 2024). A high-frequency (220 Hz) infrared camera system
161 (ViewPointEyeTracker® system, Arrington Research, Inc.) was also used to track pupil
162 size and position during the recording session.

163 Neurons' optimal orientation/direction, spatial frequency, temporal frequency,
164 size, and contrast were measured using circular drifting sinusoidal gratings. Following
165 the assessment of a neuron's response to optimal drifting grating, one of the four tuning
166 properties (orientation, spatial frequency, temporal frequency, and contrast) was
167 pseudorandomly tested while keeping the other parameters at their optimal values.
168 Each grating parameter was presented for 0.5 s to 2 s, with a 1 s gap in between.

169 Responses were classified in sustained or transient using an optimal flashing
170 stationary stimulus, which were presented on the center on RF for 2 s, with a 2 s gap
171 during the alert brain state.

172 Data analysis

173 The offline data analysis methods have been reported before (Zhuang et al.,
174 2013; Su et al., 2024) and are described briefly here. Spikes from single neurons were
175 isolated during the recording session and verified offline with Plexon cluster analysis
176 software. All data analysis was performed with NeuroExplorer (NexTechnologies, Inc.),
177 MATLAB (The MathWorks, Inc.), and Python (Python Software Foundation).

178 The spatial structure of L5 SInS' RFs was assessed using two indices: the Local
179 Similarity Index (LSI, DeAngelis et al., 1999; Usrey et al., 1999; Alonso et al., 2001) and
180 Sign Index (Jin et al., 2008; Van Hooser et al., 2013). LSI was calculated as $(RF_{ON} \cdot$
181 $RF_{OFF}) / \sqrt{(RF_{ON} \cdot RF_{ON})(RF_{OFF} \cdot RF_{OFF})}$. It quantifies the degree of spatial segregation
182 between ON (RF_{ON}) and OFF (RF_{OFF}) subfields, with a value of 0 indicating complete
183 separation and 1 indicating perfect superimposition. The Sign Index was calculated as
184 $(\sum R_{ON(i,j)} - \sum R_{OFF(i,j)}) / (\sum R_{ON(i,j)} + \sum R_{OFF(i,j)})$. $RF_{ON(i,j)}$ is the maximum response of
185 the ON subfield while the $RF_{OFF(i,j)}$ represents the maximum response of the OFF
186 subfield. Sign index evaluates the dominance of ON or OFF subfields, ranging from -1
187 for OFF-dominated to 1 for ON-dominated RFs, with values close to zero representing a
188 balance between ON and OFF polarity. SInS with a Sign Index absolute value from 0 to
189 0.3 were classified as having balanced ON-OFF subfield dominance. Cells with a Sign
190 Index absolute value from 0.3 to 0.7 were considered as having a stronger ON or OFF
191 subfield. Those with a Sign Index absolute value from 0.7 to 1 were classified as having
192 a single ON or OFF subfield. The subfield width was measured along the orientation
193 perpendicular to the cell's optimal orientation from the dominant subfield (Zhuang et al.,
194 2013; Su et al., 2024). To ensure the quality of the RFs, each single SInS was mapped at
195 least twice to confirm repeatability without any eye movement. In most cases, SInS
196 were mapped at least five times during the recording session to verify RF repeatability.
197 We selected recording files based on neuron isolation quality and the number of spikes

198 collected for further analysis. SINs that did not produce repeatable RFs due to eye
199 movement, noise, or insufficient spike count were excluded from the data set.

200 The response latency was calculated from the neurons' peristimulus time
201 histograms (PSTHs) to optimal flash stimuli. The latency is defined as the time at which
202 the PSTH was smoothed by a boxcar filter with a 30 ms sliding window, and it was
203 determined as the point when it first exceeded 40% of its maximum value (Jin et al.,
204 2011). The sustained/transiency of the neuronal response was tested using a flashed
205 stimulus optimized to the SINs' preferred polarity and size. The sustained index was
206 calculated by the ratio of the neuron's maintained response to the baseline activity when
207 the animal is alert. PSTHs were generated with a bin size of 5 ms to measure the
208 maintained response, which was defined as the mean firing rate within 0.5 s – 1.0 s
209 after stimulus onset, while baseline activity was measured as the mean firing rate from -
210 0.5 s to 0 s before stimulus onset. The alert brain state was indicated by hippocampal
211 "theta" activity (5 – 7 Hz) and desynchronized cortical EEG (Bezdudnaya et al., 2006;
212 Zhuang et al., 2013).

213 The mean firing rate (F0), first harmonic component (F1) of the PSTHs, F1/F0
214 ratios, and Fano Factors were measured from the SINs' response to the optimal drifting
215 grating stimuli. The analysis of all tuning properties followed the same methodology as
216 described earlier (Su et al., 2024). Orientation tunings were fitted by von Mises
217 distribution functions responses (Nowak et al., 2008; Zhuang et al., 2013). The
218 orientation selectivity index (OSI), and direction selectivity index (DSI) were calculated
219 as $(R_{\text{pref}} - R_{\text{orth}})/(R_{\text{pref}} + R_{\text{orth}})$, and $(R_{\text{pref}} - R_{\text{null}})/(R_{\text{pref}} + R_{\text{null}})$. Here, R_{pref}
220 denotes the neuron's response in the preferred orientation/direction, R_{orth} signifies the
221 neuron's average responses in the stimulus directions 90° away from the preferred
222 direction, and R_{null} represents the neuron's response to the opposite of the preferred
223 direction. Both measurements (OSI and DSI) have values ranging from 0 to 1, with
224 higher values meaning stronger orientation selectivity and direction selectivity,
225 respectively. Contrast tunings were tested on 8 different contrasts ranging from 1% to
226 95% (Cano et al., 2006; Zhuang et al., 2013). The F0 responses were fitted by a
227 hyperbolic model (Albrecht and Hamilton, 1982; Cano et al., 2006; Zhuang et al., 2013),
228 without high contrast suppression $y = R_0 + A * x^n / (C^n + x^n)$, or with high contrast
229 suppression: $y = R_0 + A * x^n / (C^{sn} + x^{sn})$. Here, R_0 is the baseline activity of the neuron,
230 A is the response amplitude, x is the contrast that we tested, and C is the contrast
231 generating the half-maximum response (C_{50}). Only the fitting curves with goodness of
232 fit value higher than 0.5 were included for further analysis.

233 The connectivity within simultaneously recorded pairs of LGN-L5 SINs was
234 investigated using cross-correlation analysis (Liew et al., 2021; Reid and Alonso, 1995;
235 Swadlow and Gusev, 2001; Bereshpolova et al., 2020). The crosscorrelogram depicted
236 the correlation between the count of L5 SINs spikes occurring within the ± 10 ms time
237 window (with 0.2 ms bins) and the LGN spikes. A significant peak is defined as at least
238 two out of three successive bins in the peak exceeded the 0.01 confidence level at
239 intervals of 1-4 ms (Fig. 1D). To evaluate the functional connectivity between the LGN

240 cell and the L5 SINS neurons, an efficacy value is calculated. Efficacy and contribution
241 values (Levick et al., 1972; Swadlow, 1995; Bereshpolova et al., 2020) are calculated by
242 counting the number of spikes that occurred in the L5 SINS during the short time
243 window of ± 0.6 ms from the peak (baseline subtracted) divided by the number of the
244 triggering LGN spikes (efficacy) or by the number of the L5 SINS spikes (contribution).

245 **Statistical analysis**

246 Statistical analyses were performed using MATLAB (MathWorks). The results
247 section provided details on the type of statistical test utilized. Data are provided as
248 Mean \pm SEM.

249

250 **Results:**

251 **Identifying characteristics of L5 SINS**

252 L5 SINS, like those of L4, are identified by their high frequency discharge (> 600
253 Hz) to electrical stimulation of the thalamus (Zhuang et al., 2013; Bereshpolova et al.,
254 2020; Fig. 1B). Although not a defining criterion, all SINS had spikes of short duration.
255 Figure 1C shows the distribution of the spike waveform durations (measured from
256 trough to peak) of the L5 SINS, L4 SINS (from Zhuang et al., 2013) and corticotectal
257 (CTect) neurons (from Su et al., 2024). CTect neurons were identified by their
258 antidromic activation following electrical stimulation of the SC (Bishop et al., 1962;
259 Swadlow and Weyand, 1987). The spike waveform durations of L5 SINS are very similar
260 to the spike waveform durations of L4 SINS (L5 SINS vs. L4 SINS: 0.21 ± 0.01 ms vs
261 0.19 ± 0.01 ms, Wilcoxon rank sum test, $p = 0.107$), but the waveform durations of L5
262 SINS are $\sim \frac{1}{2}$ those of the CTect neurons (0.21 ± 0.01 ms vs. 0.38 ± 0.01 ms, Wilcoxon
263 rank sum test, $p = 4.803e^{-24}$, Fig. 1C).

264 **Spatial receptive field properties of L5 SIN:**

265 We tested the spatial RFs of 65 L5 SINS to small stationary flashing light and
266 dark spots using methods of reverse correlation (Methods). The RFs of fifty-six of these
267 cells (86%) consisted of highly overlapping ON and OFF zones (Fig. 2A1). The RFs of
268 six L5 SINS consisted of a single ON (four cells, Fig. 2A2) or OFF (two cells, Fig. 2A3)
269 zone. Two L5 SINS responded to flashing spots only with suppression of spontaneous
270 firing, and one remaining cell was not driven by visual stimulation (Table 1). Two SINS
271 with suppressive RFs and one non-responsive SIN were not tested with drifting grating
272 stimulations for their visual properties, and thus are not included in most of the
273 subsequent analyses. Notably, the most common type of RF described in Fig. 2A1 (with
274 highly overlapping ON/OFF subfields) is the only type of spatial RF previously seen in
275 L4 SINS (Zhuang et al., 2013; Bereshpolova et al., 2020). The measure "Sign Index"
276 (Jin et al., 2011; Van Hooser et al., 2013; Methods) was used to quantify the strength of
277 ON and OFF subfields. Fig. 2B shows the distribution of the Sign Index values for L5
278 SINS. The majority of L5 SINS have Sign Index values around -0.3 to 0.3, indicating they

279 have roughly balanced ON and OFF responses (see Methods). The Sign Index values
280 of -1 and +1 indicate pure OFF and ON responses, respectively. Because the L5 SINS
281 are spontaneously active, there is often considerable noise in the RF plots. For this
282 reason, RFs were classified as having a single ON or OFF subfield if Sign Index values
283 were > 0.7 or < -0.7 , respectively. To quantify the degree of overlap between the ON
284 and OFF subfields, the measure “Local Similarity Index” (LSI, DeAngelis et al., 1999;
285 Usrey et al., 1999; Alonso et al., 2001, Methods) was calculated. Fig. 2C shows the
286 distribution of LSI for L5 SINS with both an ON and an OFF subfield. All of these L5
287 SINS have $LSI > 0.3$ (mean = 0.59 ± 0.02), indicating their ON and OFF subfields are
288 overlapping to some extent.

289 **Response properties of L5 SINS: Comparisons with L4 SINS**

290 In addition to their spatial RF structure, L5 SINS share many similarities with the
291 L4 SINS. Importantly, they both show nonlinear spatial summation in the responses to
292 optimal drifting sinusoidal gratings ($F1/F0$ ratio < 1). The linearity of spatial summation
293 was measured as the ratio between the modulated ($F1$) to the unmodulated ($F0$)
294 responses. A response is considered linear when the $F1/F0$ ratio > 1 , and nonlinear
295 when the ratio < 1 (Skottun et al., 1991; Movshon et al., 1978b, a; Martinez and Alonso,
296 2003; Zhuang et al., 2013). All but two L5 SINS responded to their optimal drifting
297 grating stimulation in a nonlinear manner. Fig. 3A is an example of an L5 SIN
298 responding to near-optimal drifting grating, with $F1/F0$ ratio of 0.07. The evoked $F0$
299 response increases during the stimulus presentation, but it was weakly modulated by
300 the sinusoidal drifting grating stimulation. By contrast, classic “simple” cells of L4
301 respond in a highly modulated linear manner to an optimal drifting visual grating. Fig. 3B
302 is an example of such a simple cell (in layer 4 of rabbit V1) responding to its optimal
303 visual stimulation, with $F1/F0$ ratio of 1.50. Fig. 3C shows the distribution of the $F1/F0$
304 ratio of L5 SINS, all but two of which have an $F1/F0$ ratio of < 1.0 (Fig. 3C, upper panel,
305 mean = 0.28 ± 0.03). We compare the L5 SINS to the $F1/F0$ ratio of L4 simple cells (Fig.
306 3C, lower panel, mean = 1.53 ± 0.03) that we previously studied (Zhuang et al., 2013).
307 Visual cortical neurons with $F1/F0$ values of < 1.0 are frequently classified as “complex”
308 cells and those with values > 1.0 as “simple” cells (Movshon et al., 1978b, a; Martinez
309 and Alonso, 2003; Briggs and Usrey, 2009; Hawken et al., 2020). Therefore, like the L4
310 SINS, all but two of the L5 SINS would be considered as complex cells based on this
311 classification. Notably, the spatial RF of the two L5 SINS with $F1/F0$ ratios of > 1 had
312 only a single subfield.

313 Figure 4 shows other similarities (A-E, all significant at $p > 0.05$) as well as
314 differences (F-L) between the L5 SINS and previously studied L4 SINS (from Zhuang et
315 al., 2013). Thus, the degree of spatial overlap in the ON and OFF subfields of the L5
316 and L4 SINS was similar (LSI: L5 vs L4 = 0.59 ± 0.02 vs. 0.66 ± 0.02 , Wilcoxon rank
317 sum test, $p = 0.067$, Fig. 4A, high LSI values mean greater overlap). Both populations
318 also have similarly high evoked unmodulated ($F0$) responses (L5 vs L4 = 50.52 ± 3.91
319 spks/s vs. 59.76 ± 4.20 spks/s, Wilcoxon rank sum test, $p = 0.061$, Fig. 4B) to a drifting

320 visual grating, and both display similar response reliability to optimal drifting grating
321 stimulation (Fano Factor: L5 vs L4 = 1.71 ± 0.18 vs. 1.33 ± 0.08 , Wilcoxon rank sum
322 test, $p = 0.185$, Fig. 4C, high Fano Factor values mean less reliable response). Both L4
323 and L5 SINs are also poorly tuned to stimulus direction (DSI: L5 vs L4 = 0.10 ± 0.02 vs.
324 0.15 ± 0.02 , Wilcoxon rank sum test, $p = 0.126$, Fig. 4D, high DSI values indicate
325 greater directional specificity), and both populations include cells that generate
326 sustained responses to stationary flash stimuli (sustained index: L5 vs L4 = 2.16 ± 0.42
327 vs 1.48 ± 0.19 , Wilcoxon rank sum test, $p = 0.573$, Fig. 4E, higher sustained index
328 higher values indicate greater sustained response).

329 By contrast, Fig. 4 F-L shows that some L5 SINs show significant differences in
330 some of their response properties compared to the L4 SINs. More L5 SINs than L4 SINs
331 are selective for stimulus orientation (OSI: L5 SINs vs. L4 SINs: 0.25 ± 0.02 vs. $0.16 \pm$
332 0.01 , Wilcoxon rank sum test, $p = 0.006$, Fig. 4F, higher OSI values indicate greater
333 selectivity for stimulus orientation). Both L5 and L4 SINs have relatively high
334 spontaneous activity, but the L5 SINs have significantly lower spontaneous activities
335 than L4 SINs (L5 SINs vs. L4 SINs: 14.46 ± 0.98 spks/s vs. 21.96 ± 2.18 spks/s,
336 unpaired t-test, $p = 7.718e^{-04}$, Fig. 4G). The modulated responses (F1) are less than $\frac{1}{2}$
337 the strength in L5 than in L4 SINs, (L5 SINs vs. L4 SINs: 14.10 ± 1.86 spks/s vs. 32.97
338 ± 3.73 spks/s, Wilcoxon rank sum test, $p = 1.358e^{-06}$, Fig. 4H). Although the great
339 majority of the L4 and L5 SINs respond to drifting sinusoidal gratings in a nonlinear
340 manner (F1/F0 ratio < 1 , Fig. 3), the L5 SINs have much lower F1 responses and,
341 therefore, they also have lower F1/F0 ratios than the L4 SINs (L5 SINs vs. L4 SINs:
342 0.28 ± 0.03 vs. 0.64 ± 0.04 , Wilcoxon rank sum test, $p = 1.813e^{-07}$, Fig. 4I). The L4 SINs
343 respond at short latencies to visual flash stimuli, with a median ~ 28.16 ms. However,
344 some L5 SINs respond at long latencies (L5 SINs vs. L4 SINs: 37.59 ± 3.65 ms vs.
345 28.65 ± 0.93 ms, Wilcoxon rank sum test, $p = 0.017$, Fig. 4J). Contrast sensitivity
346 measured as the contrast that elicited half of the maximum response (C50, lower values
347 indicate greater contrast sensitivity) is also lower in L5 than L4 SINs (L5 SINs vs. L4
348 SINs: 17.63 ± 2.70 % vs. 10.83 ± 1.94 %, Wilcoxon rank sum test, $p = 0.011$, Fig. 4K).
349 The RF sizes of the L5 SINs and L4 SINs are also different. The dominant subfield
350 widths are significantly smaller in L5 than L4 SINs (L5 SINs vs. L4 SINs: 6.62 ± 0.39
351 deg vs 8.35 ± 0.53 deg, Wilcoxon rank sum test, $p = 0.011$, Fig. 4L).

352 Figure 4F-L show differences between L5 and L4 SINs: F, Distribution of OSI for
353 L5 SINs and L4 SINs. The majority of L5 and L4 SINs are broadly tuned for stimulus
354 orientation, but some L5 SINs are orientation selective. G, The spontaneous activities
355 are significantly lower in L5 than L4 SINs. H, Distribution of evoked F1 responses for L5
356 and L4 SINs. The L5 SINs have lower evoked F1 responses than the L4 SINs,
357 indicating weaker modulation to optimal drifting sinusoidal gratings. I, Distribution of
358 F1/F0 ratio for L5 SINs and L4 SINs. Although L5 SINs are less modulated to optimal
359 drifting sinusoidal gratings than L4 SINs, their maximum evoked responses are similar
360 (F0 response, Fig. 4B). The F1/F0 ratio is much lower in L5 than L4 SINs. J, Distribution
361 of visual latency to flash stimuli for L5 and L4 SINs. L4 SINs respond at very short

362 latencies to flash stimuli, while some L5 SINs respond much more slowly than L4 SINs.
363 K, Distribution of contrast sensitivity measured as C50 (%) for L5 SINs and L4 SINs.
364 The L5 SINs have higher C50 values than the L4 SINs, indicating less sensitivity to
365 stimulus contrast. L, Distribution of dominant RF width for L5 SINs and L4 SINs. The L5
366 SINs have smaller dominant RF widths than the L4 SINs.

367 **L5 SIN properties related to their synaptic latencies to LGN stimulation.**

368 All of the L5 SINs studied responded to electrical stimulation of the LGN with a
369 burst of high-frequency spikes, but the latency of the first spike in this discharge differed
370 considerably among cells. Figure 5A shows the distribution of the synaptic latencies of
371 L5 SINs to electrical stimulation of the LGN (mean = 2.35 ms, range = 1.4 – 5.0 ms). As
372 described in Methods, we have estimated the depth of L5 as extending from 500 μ m –
373 800 μ m below the reversal point of the flash-evoked LFP. Fig. 5B shows that the depths
374 of the L5 SINs were loosely correlated with their synaptic latencies to thalamic
375 stimulation. SINs located in deeper L5 tended to have long synaptic latencies ($r = 0.286$,
376 $p = 0.021$). The synaptic latency of the L5 SIN was also related to visual response
377 properties. L5 SINs with longer synaptic latencies were more selective for stimulus
378 orientation ($r = 0.384$, $p = 0.012$, Fig. 5C). Fig. 5D shows visual response latency to a
379 flash stimulus, with longer visual response latencies seen in cells with longer synaptic
380 latencies to the electrical stimulus ($r = 0.493$, $p = 0.007$). L5 SINs with longer latencies
381 to the electrical stimulus have lower spontaneous firing rates ($r = -0.421$, $p = 0.001$, Fig.
382 5D) and lower response rates to optimal drifting grating stimuli ($r = -0.465$, $p = 0.001$,
383 Fig. 5E). Synaptic latency to electrical stimulation was not significantly related to their
384 linearity of spatial summation (F1/F0 ratio), modulated F1 response, direction selectivity,
385 contrast sensitivity, response reliability, or dominant RF width (figures not shown).

386 **Thalamocortical synaptic inputs and their relationship to L5 SIN response** 387 **properties**

388 It is tempting to speculate that L5 SINs responding at short synaptic latencies to
389 electrical stimulation of the LGN receive direct monosynaptic input and, conversely,
390 those responding at long latencies receive only weak or indirect multisynaptic LGN
391 input. It is well known, however, that evidence from electrical stimulation alone is not
392 sufficient to justify such conclusions since (a) the electrical stimulus may activate
393 afferents that do not originate at the stimulation site and (b) the electrical stimulus may
394 activate corticofugal fibers, generating antidromic impulses that invade collaterals that
395 synapse on and activate the cortical SINs.

396 SINs of L4 in both V1 and S1 have been shown to receive potent monosynaptic
397 thalamic inputs (Swadlow, 1995, 2002; Zhuang et al., 2013). However, LGN afferents
398 synapse much more extensively in L4 than in L5 and it is not known the extent to which
399 L5 SINs receive significant monosynaptic LGN inputs. We were interested in this
400 because the differences in visual properties (as shown in Figure 4) between L5 SINs

401 and L4 SINs could potentially be attributed to whether L5 SINs receive weaker/fewer
402 direct inputs from the LGN.

403 Here, we used cross-correlation methods to investigate whether the L5 SINs
404 receive monosynaptic inputs from the LGN, the efficacy of such inputs, and how such
405 input might relate to their response to electrical stimulation of the LGN and to their
406 visual response properties. Using this method in sensory thalamocortical systems,
407 requires achieving a precise topographic (retinotopic) alignment between the thalamic
408 and cortical neurons. Here we only investigated and further analyzed the LGN-L5 SIN
409 pairs that are in retinotopic alignment, such that the LGN and SIN RF centers were
410 separated by a distance equivalent to <80% of the diameter of the LGN RF center (see
411 Methods). Based on this criterion for retinotopic alignment, we found 13 LGN-L5 SIN
412 pairs that showed evidence of synaptic connectivity. Nineteen pairs that were
413 retinotopically aligned to an equivalent degree were not connected. Figure 6A-M shows
414 cross-correlograms of each of the LGN-L5 SIN pairs that met our criteria for
415 monosynaptic connectivity (see Methods). Each cross-correlogram shows a brief and
416 abrupt peak in SIN spike probability within 1- 4 ms after the LGN spikes (see Methods).
417 Efficacy (E) and contribution (C) values were used to quantify the strength/impact of the
418 connection and were labeled in each of the LGN-L5 SIN cross-correlogram. Note that
419 although Fig. 6 shows 13 connected LGN-L5 SIN pairs, only 10 SINs are represented
420 by this figure. This is because, in cases A and B, a single L5 SIN was studied with two
421 LGN concentric cells, one ON-centered and the other OFF-centered. Similarly, in case
422 C and D, and in case G and H, two other SINs both receive input from two different LGN
423 neurons (again, one ON-center and the other OFF-center). Our data in Fig. 6 seems to
424 indicate that LGN neurons with OFF-center RFs exhibited greater efficacy onto L5 SINs.
425 However, these data include one OFF-center LGN neuron that made synaptic contact
426 with four L5 SINs (connections depicted in Fig. 6A, C, E, and I are from the same LGN
427 off-center neuron). Due to the over-representation of this single LGN neuron in our
428 sample, our dataset remains too limited to conclude whether LGN neurons with off-
429 center RFs provide stronger input to L5 SINs compared to LGN cells with on-center
430 RFs.

431 All of the connected L5 SINs were recorded between 520 and 650 μm beneath
432 the reversal point of the flash evoked potential (Fig. 6N, right column). Moreover, most
433 were recorded very near to CTect neurons, which, in rabbits, are predominantly found in
434 the superficial $\frac{1}{2}$ of layer 5 (Su et al., 2024; Swadlow and Weyand, 1981). Thus, seven
435 of the 10 connected L5 SINs were recorded either simultaneously with a CTect neuron,
436 sequentially within 60 μm of a CTect neuron, or $\sim 200 \mu\text{m}$ below a CTect neuron using
437 the same electrode during a single penetration. This provided additional evidence, aside
438 from the depth profile, that these SINs are located in L5. Although the other three
439 connected L5 SINs were not recorded with a CTect in the same penetration, they were
440 all located near the middle of L5 (Fig. 6N, open circles). Therefore, the existence of
441 CTect neurons in close proximity to the monosynaptically connected SINs with LGN
442 affirmed the location of these SINs in L5.

443 Next, we asked whether the response properties of the 10 LGN-connected SINs
444 differed from the properties of the 19 SINs that, according to our cross-correlation
445 analysis, were not connected despite being retinotopically aligned to an equal degree.

446 We observed the following differences between LGN-connected vs. non-
447 connected L5 SINs that were aligned to an equal degree: (1) the cortical depth at which
448 they were found, (2) the amplitude of the LGN spike-triggered LFP (triggered by spikes
449 of the single LGN cell under study, Methods) in the vicinity of the SIN, (3) the
450 spontaneous activity of the SINs, and (4) their synaptic latencies to LGN electrical
451 stimulation. Thus, the L5 SINs that received monosynaptic LGN input were all located in
452 the upper half of L5, while none of the L5 SINs located in the lower half of L5 received
453 monosynaptic LGN input (depth: connected vs. not connected: $573 \pm 17 \mu\text{m}$ vs. $693 \pm$
454 $19 \mu\text{m}$, unpaired t-test, $p = 1.369e^{-04}$, Fig. 7A). The amplitude of LGN spike-triggered
455 LFP at the vicinity of the connected L5 SINs is ~ 6 times higher than the amplitude of
456 the spike-triggered LFP near the non-connected L5 SINs (connected vs. not connected:
457 $10.00 \pm 2.37 \mu\text{V}$ vs. $1.47 \pm 0.51 \mu\text{V}$, Wilcoxon rank sum test, $p = 4.067e^{-04}$, Fig. 7B).
458 Also, the LGN connected L5 SINs have higher spontaneous activity than those of the
459 non-connected L5 SINs (connected vs. not connected: $18.01 \pm 1.62 \text{ spks/s}$ vs. $10.76 \pm$
460 1.34 spks/s , unpaired t-test, $p = 0.003$, Fig. 7C). All connected L5 SINs have short (\leq
461 2.4 ms) synaptic latency to thalamic electrical stimulation (indicative of monosynaptic
462 activation, Bereshpolova et al., 2020), while the synaptic latency of the non-connected
463 L5 SINs can be much longer (connected vs. not connected: $2.02 \pm 0.08 \text{ ms}$ vs. $2.76 \pm$
464 0.31 ms , unpaired t-test, $p = 0.041$, Fig. 7D).

465 **Discussion (1500 words, 1500 words limit)**

466 Fast-spike interneurons are found throughout sensory neocortex, comprising
467 about $\frac{1}{2}$ of the inhibitory neurons in many cortical areas (Rudy et al., 2011; Tamamaki
468 et al., 2003). These parvalbumin-expressing interneurons are morphologically and
469 biochemically distinct from neighboring excitatory cells, and from other classes of
470 GABAergic interneurons (Markram et al., 2004; McBain and Fisahn, 2001; Tremblay et
471 al., 2016). They are also physiologically distinct from excitatory neurons, displaying
472 short-duration action potentials, high firing rates, and distinct RF properties (Simons,
473 1978; Swadlow, 1988, 1989, 1990, 1991; Hirsch et al., 2003; Nowak et al., 2008). They
474 also respond potently to thalamocortical inputs and generate fast and powerful local
475 feed-forward inhibition (Gibson et al., 1999; Cruikshank et al., 2007; Porter et al., 2001;
476 Swadlow, 2003).

477 Cross-correlation studies in L4 barrel cortex of rats and awake rabbits (Bruno
478 and Simons, 2002; Swadlow and Gusev, 2001) have shown that fast-spike
479 neurons/SINs receive a highly convergent synaptic input that drives many neurons (\sim
480 60%) in the aligned thalamic “barreloid”. Notably, although most neighboring spiny
481 neurons in L4 are sharply tuned to the direction of whisker displacement, fast spike
482 neurons/SINs are very broadly tuned, despite considerable directional selectivity in their
483 thalamic afferents. This broad tuning is thought to result from strong convergence of

484 many thalamic neurons with a broad range of directional preferences onto the
485 interneurons (Alonso and Swadlow, 2005; Swadlow, 2003; Swadlow et al., 2005b). In
486 rabbit V1, a similar unselective convergence of LGN neurons onto L4 SINS occurs
487 (Bereshpolova et al., 2020). Like SINS of L4 barrel cortex, SINS of L4 in V1 are very
488 broadly tuned to some stimulus parameters (visual stimulus direction and orientation),
489 and the observed high degree of thalamocortical convergence is thought to be related to
490 these broad tuning characteristics (Zhuang et al., 2013).

491 L5 of V1 also has many fast-spike interneurons that potently inhibit their
492 neighbors (Xiang et al., 2002). However, the axonal arborization and synaptic drive of
493 LGN axons in L5 is considerably sparser than in L4 (Humphrey et al., 1985; Ji et al.,
494 2016; Stoelzel et al., 2008; Zhuang et al., 2021). Moreover, L5 receives strong input
495 from superficial cortical layers and these inputs, have been posited to contribute
496 strongly to sensory response properties of L5 neurons (Gilbert and Wiesel, 1983;
497 Douglas and Martin, 2004). Therefore, it is reasonable to suspect that SINS of L5 and
498 L4 might have different response properties, and that these differences might be related
499 to differences in thalamocortical connectivity. Indeed, we found both similarities and
500 differences in response properties of L5 and L4 SINS, and argue that some of these
501 differences are related to differences in thalamocortical connectivity.

502 **RF properties of L5 vs. L4 SINS**

503 (1) Response linearity: both L5 and L4 SINS show non-linear responses to near-
504 optimal drifting sinusoidal gratings ($F1/F0$ ratios <1 ; Skottun et al., 1991), responding
505 with a weakly modulated increase in firing rate. Such non-linear responding is similar to
506 that seen in closely neighboring L5 CTect neurons (Su et al., 2024), but very different
507 from the pronounced linear spatial summation of L4 simple cells (Zhuang et al., 2013).
508 Classification of visual cortical neurons into “simple” or “complex” is commonly
509 determined by the $F1/F0$ ratio (Movshon et al., 1978a, b; Carandini et al., 1997; Ringach
510 et al., 2002). Thus, *nearly all of the SINS in both L4 and L5*, including all but two of the
511 very few SINS in L5 with a single subfield, would be classified as “complex” according to
512 this criterion.

513 (2) Spatial RFs: Highly overlapping ON/OFF subfields were found in *all* L4 SINS,
514 and in the great majority (86%) of L5 SINS. However, 6 of the L5 SINS had only a single
515 ON or OFF subfield, a RF characteristic not seen in L4 SINS.

516 (3) Orientation selectivity: Both L5 and L4 SINS displayed minimal directional
517 selectivity. Orientation tuning was also relatively poor for both L5 and L4 SINS, when
518 compared to that of simple cells of L4 (Zhuang et al., 2013) or CTect cells of L5 (Su et
519 al., 2024). However, some L5 SINS were better tuned for stimulus orientation than any
520 of the L4 SINS (Fig. 4F). As discussed below, we believe this is due to a different
521 balance of thalamocortical and corticocortical inputs to these cells.

522 (4) Spontaneous and visually driven firing rates: In multiple sensory and motor
523 cortical areas of awake rabbits, SINS have the highest spontaneous firing rates studied

524 (Swadlow, 1988, 1989, 1990, 1991, 1994). While L5 V1 SInS have high rates of
525 spontaneous activity compared to neighboring CTect neurons in L5 (Su et al., 2024),
526 firing rates are significantly lower in L5 than L4 SInS (Fig. 4G). Unmodulated visually
527 driven rates (F0) of L4 and L5 SInS are very similar (Fig. 4B), but, because the
528 modulated visually driven rates (F1) are so low in the L5 SInS, their F1/F0 ratios are
529 also lower than in L4 SInS.

530 (5) Latency to visual stimulation: Response latencies to visual stimuli were
531 significantly longer in L5 SInS than in L4 SInS (Fig. 4J). Such a laminar difference in
532 response latencies is consistent with a “canonical cortical circuit” (Gilbert and Wiesel,
533 1983; Douglas and Martin, 1991, 2004) in which sensory information reaches L5 largely
534 through an indirect pathway (thalamus to L4 to L2/3 to L5). Such a pathway would result
535 in a longer latency to sensory stimulation in L5. Although the canonical circuit has been
536 challenged by some studies (e.g., Constantinople and Bruno, 2013; Pluta et al., 2015),
537 as noted above, L5 does receive fewer thalamic afferents, and more input from
538 superficial layers than L4. Therefore, some (if not all) long latency responses mediated
539 by superficial inputs would be expected.

540 **RF properties of L5 SInS are related to thalamocortical inputs**

541 Two complementary methods were used to infer thalamocortical connectivity
542 (Swadlow and Lukatela, 1996): electrical stimulation of the LGN, and cross-correlation
543 of retinotopically aligned LGN-SIn cell pairs. LGN stimulation will activate neurons that
544 receive monosynaptic LGN input at a latency consistent with (a) the thalamocortical
545 axonal conduction times (0.8 – 2 ms, for the great majority of LGN axons (Swadlow and
546 Weyand, 1985; Stoelzel et al., 2008) plus the synaptic delay. However, LGN stimulation
547 may be subthreshold for driving postsynaptic spikes. Moreover, thalamic stimulation can
548 also synaptically activate cortical neurons by stimulating thalamocortical axons
549 originating in nearby thalamic nuclei (e.g., the pulvinar, Weyand and Swadlow, 1986), or
550 by antidromically activating corticofugal axons that pass near the thalamic stimulation
551 site, resulting in antidromic invasion of the corticofugal axonal recurrent axon collaterals
552 that synapse in the cortex. Therefore, while a short synaptic latency (e.g., < 3 ms) in a
553 cortical neuron following LGN stimulation is suggestive of monosynaptic LGN input, and
554 a longer synaptic latency is suggestive of polysynaptic input, such results are not
555 definitive.

556 By contrast, cross-correlation analysis showed definitively, and for the first time,
557 that many L5 SInS receive potent monosynaptic input from the LGN. Synaptic efficacies
558 were in some cases extremely high; (e.g., Fig. 6A, 6C). While extracellular cross-
559 correlation analysis cannot detect subthreshold inputs, or polysynaptic inputs, it is
560 definitive in detection of strong monosynaptic inputs (Moore et al., 1970; Swadlow and
561 Lukatela, 1996). Together, the methods of electrical stimulation of the thalamus, and
562 cross-correlation of aligned LGN-SIn neuronal pairs provided results consistent with the
563 idea that L5 SInS that display short latencies to thalamic stimulation are receiving
564 monosynaptic input from the LGN, and have properties more similar to L4 SInS. Our

565 results also indicate that there is no evidence of L5 SINs with longer synaptic latencies
566 receiving monosynaptic thalamic input. Instead, they appear to be receiving indirect
567 (multisynaptic) LGN input, possibly mediated by superficial cortical layers. Thus, the L5
568 SINs responding at longer synaptic latencies to thalamic stimulation displayed greater
569 orientation selectivity than either the short-latency L5 SINs or the L4 SINs (as do most
570 projection cells found in L2/3, Swadlow, 1988), and responded at longer latencies to
571 visual stimulation (also consistent with a multisynaptic pathway). Long latency L5 SINs
572 also had lower spontaneous and visually driven firing rates, and they were deeper in L5
573 than were the short latency SINs. Importantly, we found that L5 SINs that received
574 monosynaptic input from their retinotopically aligned LGN neuron (based on cross-
575 correlation analysis) also responded to the LGN electrical stimulation at short latencies
576 (< 2.5 ms). These LGN “connected” SINs were only found in the superficial $\frac{1}{2}$ of L5 and
577 had spontaneous firing rates considerably higher than those of non-connected SINs (C
578 vs. NC in Fig. 7).

579 **Conclusions**

580 Despite the very different morphology and connectivity of L4 and L5 in
581 mammalian neocortex, L5 SINs display remarkable similarities with SINs of L4,
582 including response non-linearity, largely overlapping ON/OFF spatial subfields, and a
583 wide variety of visual response properties. L5 SINs also differed in a number of respects
584 from L4 SINs, and some of these differences are related to the presence of
585 monosynaptic LGN inputs that we demonstrate in L5 SINs for the first time.
586 Investigating the role of thalamocortical (and other) inputs in the synthesis of sensory
587 response properties of these neurons is crucial to understand the functional diversity of
588 fast-spike inhibitory interneurons in different layers of sensory neocortex.

589

590 **Figure captions**

591 Figure 1. General methods. A, Schematic of stimulating and recording electrode
592 placement in experimental preparation. Spikes were recorded from LGN neurons and
593 from cortical L5 SINs. The same cortical electrode used to record the L5 SIN spikes was
594 used to record local field potentials and to compute spike-triggered LFPs (st-LFPs)
595 elicited by LGN spikes (Jin et al., 2008; Swadlow and Gusev, 2000; Stoelzel et al.,
596 2008). Stimulation electrodes were implanted in LGN to identify SINs. B, SINs were
597 identified with at least 3 spikes with minimum interspike interval (ISI) < 1.667 ms to
598 electrical stimulation. C, Distribution of the spike waveform duration of the L5 SINs, L4
599 SINs (from Zhuang et al., 2013) and CTect neurons (from Su et al., 2024), measuring
600 from trough to peak. D, An example of cross-correlogram between an LGN neuron and
601 an L5 SIN. The depth of L5 SIN recording site, efficacy (E), and contribution (C) are
602 shown on the upper left of the cross-correlogram. The retinotopic alignment between
603 the LGN neuron with an OFF-center concentric RF (blue oval contour shows the center

604 position) and the L5 SIN RFs (red: ON response, blue: OFF response) are shown on
605 the left side of the cross-correlogram as well.

606 Figure 2. Spatial RF structures of the L5 SINs. A1, The majority (86%) of L5 SINs have
607 highly overlapping ON-OFF subfields. Left, heat maps for SIN responses to light stimuli
608 (for ON subfield) and dark stimuli (for OFF subfield). Right, spatial RF map for the cell.
609 Red, ON subfield; Blue, OFF subfield. A2-A3, A few L5 SINs have a single ON or OFF
610 subfield. B, Distribution of Sign Index. The majority of L5 SINs have Sign Index values
611 close to 0, indicating balanced ON and OFF subfields. Two SINs have Sign Index $< -$
612 0.7 , and therefore were classified as having a single OFF subfield. Four SINs have Sign
613 Index > 0.7 and were classified as having a single ON subfield. C, Distribution of Local
614 Similarity Index (LSI) of L5 SINs with both an ON and an OFF subfield. LSI was not
615 measured for the SINs with a single subfield. The L5 SINs have highly overlapped ON
616 and OFF subfields. The red and blue circles illustrate ON and OFF subfields are
617 completely separated when LSI = 0 or are completely overlapped when LSI = 1. For
618 those six L5 SINs with a single subfield, their LSIs were not calculated.

619 Figure 3. L5 SINs, like SINs of L4, respond in a nonlinear manner to a near-optimal
620 drifting visual grating. A, An example of an L5 SIN responding to its optimal drifting
621 sinusoidal grating in a nonlinear manner with a $F1/F0$ ratio < 1 . B, An example of an L4
622 simple cell responding to its optimal drifting sinusoidal grating in a linear manner, with
623 $F1/F0$ ratio > 1 . C, Distributions of $F1/F0$ ratio for L5 SINs (upper panel) and L4 simple
624 cells (lower panel). All but two of the L5 SINs have $F1/F0$ ratio < 1 , thus they are
625 considered to have unmodulated response and can be classified as complex cells
626 according to their nonlinear responses (Movshon et al., 1978a; Skottun et al., 1991). By
627 contrast, the great majority of L4 simple cells (as defined by their spatial RF structure,
628 Zhuang et al., 2013) have an $F1/F0$ ratio > 1 , thus they have a modulated response and
629 can also be classified as simple cells according to their linear responses (Movshon et
630 al., 1978b; Skottun et al., 1991).

631 Figure 4. Similarities (A-E) and differences (F-L) between L5 SINs and previously
632 studied L4 SINs: A, Distributions of LSI for L5 SINs and L4 SINs. High LSI values mean
633 greater overlap between ON and OFF subfields. B, Distributions of maximum evoked $F0$
634 responses for L5 SINs and L4 SINs measured with their optimal drifting grating
635 stimulation. C, Distribution of Fano Factor for L5 SINs and L4 SINs. Fano Factor was
636 used to measure the respond reliability of the cells. Fano factors are lowest in cells that
637 respond most reliably to visual stimuli. D, Distribution of directional selective index (DSI)
638 for L5 SINs and L4 SINs. Both L5 and L4 SINs have low values of DSI, indicating poor
639 selectivity for stimulus direction. E, Distribution of sustained index for L5 and L4 SINs.

640 Figure 5. Synaptic latency to LGN stimulation is related to visual properties. A,
641 Distribution of synaptic latency for all L5 SINs. B, The depth of the L5 SINs is loosely
642 correlated with their synaptic latency. Black dots represent individual L5 SINs, while four
643 red dots indicate average depths for SINs with latencies ranging from 1-2 ms, 2-3 ms, 3-
644 4 ms, and 4-5 ms, with vertical red lines indicating the standard error of the mean for the

645 average depths. The cells located deeper in the L5 tend to have longer synaptic latency.
646 The label indicating Pearson's $r = 0.286$ and $p\text{-value} = 0.021$ is based on the raw data
647 (represented by black dots). While Pearson's $r = 0.981$ and $p\text{-value} = 0.019$ are based
648 on the averaged depths for SINs across different synaptic latency ranges (red dots, r
649 and p values are not shown on the figure). C, The synaptic latencies of L5 SINs are
650 correlated with orientation selectivity, SINs with longer synaptic latency are more tuned
651 for stimulus orientation. D, The synaptic latencies of L5 SINs to electrical stimulation of
652 the LGN are correlated with visual latencies to flash stimulation. SINs with longer
653 synaptic latency respond at longer latencies to visual flash stimulation. E – F, The
654 synaptic latencies of L5 SINs to electrical stimulation of the LGN are correlated with the
655 spontaneous and evoked F0 activities. SINs with longer synaptic latency have lower
656 spontaneous activity and lower evoked F0 activity.

657 Figure 6. L5 SINs received monosynaptic LGN inputs. A-M, LGN-L5 SIN cross-
658 correlograms organized in descending sequence of their efficacy values. Retinotopic
659 alignment between LGN and L5 SINs RF maps are showed above each cross-
660 correlogram. The horizontal bars below the RF maps represent a length of 2 degrees.
661 Each of the SINs is labeled with respect to the reversal point of the flash-evoked
662 potential. Efficacy (E) and contribution (C) of each pair connection are listed below their
663 RFs. Three SINs received convergent input from two different LGN neurons. A-B, An L5
664 SIN received convergent inputs from one OFF concentric LGN neuron (A), and one ON
665 concentric LGN neuron (B). C-D, Another L5 SIN received convergent inputs from one
666 OFF concentric LGN neuron (C), and one ON concentric LGN neuron (D). G-H, A third
667 SIN received convergent inputs from one OFF concentric LGN neuron (G), and one ON
668 concentric LGN neuron (H). N, Depth distribution of L5 SINs recorded relative to the
669 location of CTect neurons (N, right column). The SINs (solid dots) were recorded either
670 simultaneously with a CTect neuron, sequentially within $60\ \mu\text{m}$ of a CTect neuron, or \sim
671 $200\ \mu\text{m}$ below a CTect neuron using the same electrode during a single penetration.
672 Three SINs (open dots) were not recorded simultaneously with a CTect neuron. The
673 depth of the CTect neurons recorded with these seven SINs is shown in the left column
674 (green dots).

675 Figure 7. Differences between the L5 SINs receiving monosynaptic LGN inputs versus
676 those, with similar retinotopic alignment, that do not receive monosynaptic LGN inputs.
677 A, The connected L5 SINs (C) were located more superficially than those L5 SINs that
678 did not receive monosynaptic LGN input (NC). B, The spike-triggered LFPs near the
679 connected L5 SINs (recorded through the same microelectrode) were significantly
680 stronger than the spike-triggered LFPs near the L5 SINs that did not receive
681 monosynaptic LGN input. C, The connected L5 SINs have significantly higher
682 spontaneous activity than the non-connected L5 SINs. D, The connected L5 SINs all
683 responded very fast to thalamic electrical stimulation compared to the non-connected L5
684 SINs.

685

686 **References:**

- 687 Albrecht DG, Hamilton DB (1982) Striate cortex of monkey and cat: contrast response function.
688 J Neurophysiol 48:217-237.
- 689 Alonso JM, Usrey WM, Reid RC (2001) Rules of connectivity between geniculate cells and
690 simple cells in cat primary visual cortex. J Neurosci 21:4002-4015.
- 691 Alonso JM, Swadlow HA (2005) Thalamocortical specificity and the synthesis of sensory cortical
692 receptive fields. J Neurophysiol 94:26-32.
- 693 Bereshpolova Y, Stoelzel CR, Gusev AG, Bezdudnaya T, Swadlow HA (2006) The impact of a
694 corticotectal impulse on the awake superior colliculus. J Neurosci 26:2250-2259.
- 695 Bereshpolova Y, Hei X, Alonso JM, Swadlow HA (2020) Three rules govern thalamocortical
696 connectivity of fast-spike inhibitory interneurons in the visual cortex. Elife 9.
- 697 Bezdudnaya T, Cano M, Bereshpolova Y, Stoelzel CR, Alonso JM, Swadlow HA (2006)
698 Thalamic burst mode and inattention in the awake LGNd. Neuron 49:421-432.
- 699 Bishop PO, Burke W, Davis R (1962) Single-unit recording from antidromically activated optic
700 radiation neurones. J Physiol 162:432-450.
- 701 Briggs F, Usrey WM (2009) Parallel processing in the corticogeniculate pathway of the macaque
702 monkey. Neuron 62:135-146.
- 703 Bruno RM, Simons DJ (2002) Feedforward mechanisms of excitatory and inhibitory cortical
704 receptive fields. J Neurosci 22:10966-10975.
- 705 Cano M, Bezdudnaya T, Swadlow HA, Alonso JM (2006) Brain state and contrast sensitivity in
706 the awake visual thalamus. Nat Neurosci 9:1240-1242.
- 707 Carandini M, Heeger DJ, Movshon JA (1997) Linearity and normalization in simple cells of the
708 macaque primary visual cortex. J Neurosci 17:8621-8644.
- 709 Constantinople CM, Bruno RM (2013) Deep cortical layers are activated directly by thalamus.
710 Science 340:1591-1594.
- 711 Cruikshank SJ, Lewis TJ, Connors BW (2007) Synaptic basis for intense thalamocortical
712 activation of feedforward inhibitory cells in neocortex. Nat Neurosci 10:462-468.
- 713 DeAngelis GC, Ghose GM, Ohzawa I, Freeman RD (1999) Functional micro-organization of
714 primary visual cortex: receptive field analysis of nearby neurons. J Neurosci 19:4046-
715 4064.
- 716 Douglas RJ, Martin KA (1991) A functional microcircuit for cat visual cortex. J Physiol 440:735-
717 769.
- 718 Douglas RJ, Martin KA (2004) Neuronal circuits of the neocortex. Annu Rev Neurosci 27:419-
719 451.
- 720 El-Boustani S, Sermet BS, Foustoukos G, Oram TB, Yizhar O, Petersen CCH (2020)
721 Anatomically and functionally distinct thalamocortical inputs to primary and secondary
722 mouse whisker somatosensory cortices. Nat Commun 11:3342.
- 723 Ferster D, Miller KD (2000) Neural mechanisms of orientation selectivity in the visual cortex.
724 Annu Rev Neurosci 23:441-471.
- 725 Gabernet L, Jadhav SP, Feldman DE, Carandini M, Scanziani M (2005) Somatosensory
726 integration controlled by dynamic thalamocortical feed-forward inhibition. Neuron 48:315-
727 327.
- 728 Gibson JR, Beierlein M, Connors BW (1999) Two networks of electrically coupled inhibitory
729 neurons in neocortex. Nature 402:75-79.
- 730 Gilbert CD, Wiesel TN (1983) Functional organization of the visual cortex. Prog Brain Res
731 58:209-218.
- 732 Hawken MJ, Shapley RM, Disney AA, Garcia-Marin V, Henrie A, Henry CA, Johnson EN, Joshi
733 S, Kelly JG, Ringach DL, Xing D (2020) Functional Clusters of Neurons in Layer 6 of
734 Macaque V1. J Neurosci 40:2445-2457.

735 Hirsch JA, Martinez LM, Pillai C, Alonso JM, Wang Q, Sommer FT (2003) Functionally distinct
736 inhibitory neurons at the first stage of visual cortical processing. *Nat Neurosci* 6:1300-
737 1308.

738 Humphrey AL, Sur M, Uhrich DJ, Sherman SM (1985) Projection patterns of individual X- and
739 Y-cell axons from the lateral geniculate nucleus to cortical area 17 in the cat. *J Comp*
740 *Neurol* 233:159-189.

741 Ji XY, Zingg B, Mesik L, Xiao Z, Zhang LI, Tao HW (2016) Thalamocortical Innervation Pattern
742 in Mouse Auditory and Visual Cortex: Laminar and Cell-Type Specificity. *Cereb Cortex*
743 26:2612-2625.

744 Jin J, Wang Y, Lashgari R, Swadlow HA, Alonso JM (2011) Faster thalamocortical processing
745 for dark than light visual targets. *J Neurosci* 31:17471-17479.

746 Jin JZ, Weng C, Yeh CI, Gordon JA, Ruthazer ES, Stryker MP, Swadlow HA, Alonso JM (2008)
747 On and off domains of geniculate afferents in cat primary visual cortex. *Nat Neurosci*
748 11:88-94.

749 Jones JP, Palmer LA (1987) The two-dimensional spatial structure of simple receptive fields in
750 cat striate cortex. *J Neurophysiol* 58:1187-1211.

751 Levick WR, Cleland BG, Dubin MW (1972) Lateral geniculate neurons of cat: retinal inputs and
752 physiology. *Invest Ophthalmol* 11:302-311.

753 Liew YJ, Pala A, Whitmire CJ, Stoy WA, Forest CR, Stanley GB (2021) Inferring thalamocortical
754 monosynaptic connectivity in vivo. *J Neurophysiol* 125:2408-2431.

755 Markram H, Toledo-Rodriguez M, Wang Y, Gupta A, Silberberg G, Wu C (2004) Interneurons of
756 the neocortical inhibitory system. *Nat Rev Neurosci* 5:793-807.

757 Martinez LM, Alonso JM (2003) Complex receptive fields in primary visual cortex. *Neuroscientist*
758 9:317-331.

759 McBain CJ, Fisahn A (2001) Interneurons unbound. *Nat Rev Neurosci* 2:11-23.

760 Moore GP, Segundo JP, Perkel DH, Levitan H (1970) Statistical signs of synaptic interaction in
761 neurons. *Biophys J* 10:876-900.

762 Movshon JA, Thompson ID, Tolhurst DJ (1978a) Receptive field organization of complex cells in
763 the cat's striate cortex. *J Physiol* 283:79-99.

764 Movshon JA, Thompson ID, Tolhurst DJ (1978b) Spatial summation in the receptive fields of
765 simple cells in the cat's striate cortex. *J Physiol* 283:53-77.

766 Nowak LG, Sanchez-Vives MV, McCormick DA (2008) Lack of orientation and direction
767 selectivity in a subgroup of fast-spiking inhibitory interneurons: cellular and synaptic
768 mechanisms and comparison with other electrophysiological cell types. *Cereb Cortex*
769 18:1058-1078.

770 Petreanu L, Huber D, Sobczyk A, Svoboda K (2007) Channelrhodopsin-2-assisted circuit
771 mapping of long-range callosal projections. *Nat Neurosci* 10:663-668.

772 Pluta S, Naka A, Veit J, Telian G, Yao L, Hakim R, Taylor D, Adesnik H (2015) A direct
773 translaminar inhibitory circuit tunes cortical output. *Nat Neurosci* 18:1631-1640.

774 Porter JT, Johnson CK, Agmon A (2001) Diverse types of interneurons generate thalamus-
775 evoked feedforward inhibition in the mouse barrel cortex. *J Neurosci* 21:2699-2710.

776 Quiquempoix M, Fayad SL, Boutourlinsky K, Leresche N, Lambert RC, Bessaih T (2018) Layer
777 2/3 Pyramidal Neurons Control the Gain of Cortical Output. *Cell Rep* 24:2799-2807
778 e2794.

779 Reid RC, Alonso JM (1995) Specificity of monosynaptic connections from thalamus to visual
780 cortex. *Nature* 378:281-284.

781 Ringach DL, Shapley RM, Hawken MJ (2002) Orientation selectivity in macaque V1: diversity
782 and laminar dependence. *J Neurosci* 22:5639-5651.

783 Rudy B, Fishell G, Lee S, Hjerling-Leffler J (2011) Three groups of interneurons account for
784 nearly 100% of neocortical GABAergic neurons. *Dev Neurobiol* 71:45-61.

785 Simons DJ (1978) Response properties of vibrissa units in rat SI somatosensory neocortex. *J*
786 *Neurophysiol* 41:798-820.

787 Skottun BC, De Valois RL, Grosf DH, Movshon JA, Albrecht DG, Bonds AB (1991) Classifying
788 simple and complex cells on the basis of response modulation. *Vision Res* 31:1079-
789 1086.

790 Stoelzel CR, Bereshpolova Y, Gusev AG, Swadlow HA (2008) The impact of an LGNd impulse
791 on the awake visual cortex: synaptic dynamics and the sustained/transient distinction. *J*
792 *Neurosci* 28:5018-5028.

793 Stoelzel CR, Bereshpolova Y, Alonso JM, Swadlow HA (2017) Axonal Conduction Delays, Brain
794 State, and Corticogeniculate Communication. *J Neurosci* 37:6342-6358.

795 Su C, Mendes-Platt RF, Alonso JM, Swadlow HA, Bereshpolova Y (2024) Visual Corticotectal
796 Neurons in Awake Rabbits: Receptive Fields and Driving Monosynaptic Thalamocortical
797 Inputs. *J Neurosci* 44.

798 Sun QQ, Huguenard JR, Prince DA (2006) Barrel cortex microcircuits: thalamocortical
799 feedforward inhibition in spiny stellate cells is mediated by a small number of fast-spiking
800 interneurons. *J Neurosci* 26:1219-1230.

801 Swadlow HA, Weyand TG (1981) Efferent systems of the rabbit visual cortex: laminar
802 distribution of the cells of origin, axonal conduction velocities, and identification of axonal
803 branches. *J Comp Neurol* 203:799-822.

804 Swadlow HA, Weyand TG (1985) Receptive-field and axonal properties of neurons in the dorsal
805 lateral geniculate nucleus of awake unparalyzed rabbits. *J Neurophysiol* 54:168-183.

806 Swadlow HA, Weyand TG (1987) Corticogeniculate neurons, corticotectal neurons, and
807 suspected interneurons in visual cortex of awake rabbits: receptive-field properties,
808 axonal properties, and effects of EEG arousal. *J Neurophysiol* 57:977-1001.

809 Swadlow HA (1988) Efferent neurons and suspected interneurons in binocular visual cortex of
810 the awake rabbit: receptive fields and binocular properties. *J Neurophysiol* 59:1162-
811 1187.

812 Swadlow HA (1989) Efferent neurons and suspected interneurons in S-1 vibrissa cortex of the
813 awake rabbit: receptive fields and axonal properties. *J Neurophysiol* 62:288-308.

814 Swadlow HA (1990) Efferent neurons and suspected interneurons in S-1 forelimb representation
815 of the awake rabbit: receptive fields and axonal properties. *J Neurophysiol* 63:1477-
816 1498.

817 Swadlow HA (1991) Efferent neurons and suspected interneurons in second somatosensory
818 cortex of the awake rabbit: receptive fields and axonal properties. *J Neurophysiol*
819 66:1392-1409.

820 Swadlow HA (1994) Efferent neurons and suspected interneurons in motor cortex of the awake
821 rabbit: axonal properties, sensory receptive fields, and subthreshold synaptic inputs. *J*
822 *Neurophysiol* 71:437-453.

823 Swadlow HA (1995) Influence of VPM afferents on putative inhibitory interneurons in S1 of the
824 awake rabbit: evidence from cross-correlation, microstimulation, and latencies to
825 peripheral sensory stimulation. *J Neurophysiol* 73:1584-1599.

826 Swadlow HA, Lukatela K (1996) Cross-correlation and microstimulation: complementary tools in
827 the extracellular analysis of synaptic interactions. *J Neurosci Methods* 64:219-225.

828 Swadlow HA, Gusev AG (2000) The influence of single VB thalamocortical impulses on barrel
829 columns of rabbit somatosensory cortex. *J Neurophysiol* 83:2802-2813.

830 Swadlow HA, Gusev AG (2001) The impact of 'bursting' thalamic impulses at a neocortical
831 synapse. *Nat Neurosci* 4:402-408.

832 Swadlow HA (2002) Thalamocortical control of feed-forward inhibition in awake somatosensory
833 'barrel' cortex. *Philos Trans R Soc Lond B Biol Sci* 357:1717-1727.

834 Swadlow HA (2003) Fast-spike interneurons and feedforward inhibition in awake sensory
835 neocortex. *Cereb Cortex* 13:25-32.

836 Swadlow HA, Bereshpolova Y, Bezdudnaya T, Cano M, Stoelzel CR (2005a) A multi-channel,
837 implantable microdrive system for use with sharp, ultra-fine "Reitboeck" microelectrodes.
838 J Neurophysiol 93:2959-2965.

839 Swadlow HA, Bezdudnaya T, Gusev AG (2005b) Spike timing and synaptic dynamics at the
840 awake thalamocortical synapse. Prog Brain Res 149:91-105.

841 Tamamaki N, Yanagawa Y, Tomioka R, Miyazaki J, Obata K, Kaneko T (2003) Green
842 fluorescent protein expression and colocalization with calretinin, parvalbumin, and
843 somatostatin in the GAD67-GFP knock-in mouse. J Comp Neurol 467:60-79.

844 Tremblay R, Lee S, Rudy B (2016) GABAergic Interneurons in the Neocortex: From Cellular
845 Properties to Circuits. Neuron 91:260-292.

846 Usrey WM, Reppas JB, Reid RC (1999) Specificity and strength of retinogeniculate
847 connections. J Neurophysiol 82:3527-3540.

848 Van Hooser SD, Roy A, Rhodes HJ, Culp JH, Fitzpatrick D (2013) Transformation of receptive
849 field properties from lateral geniculate nucleus to superficial V1 in the tree shrew. J
850 Neurosci 33:11494-11505.

851 Weyand TG, Swadlow HA (1986) Thalamic inputs to visual areas 1 and 2 in the rabbit. J Comp
852 Neurol 250:521-528.

853 Xiang Z, Huguenard JR, Prince DA (2002) Synaptic inhibition of pyramidal cells evoked by
854 different interneuronal subtypes in layer v of rat visual cortex. J Neurophysiol 88:740-
855 750.

856 Zarrinpar A, Callaway EM (2016) Functional Local Input to Layer 5 Pyramidal Neurons in the
857 Rat Visual Cortex. Cereb Cortex 26:991-1003.

858 Zhuang J, Stoelzel CR, Bereshpolova Y, Huff JM, Hei X, Alonso JM, Swadlow HA (2013) Layer
859 4 in primary visual cortex of the awake rabbit: contrasting properties of simple cells and
860 putative feedforward inhibitory interneurons. J Neurosci 33:11372-11389.

861 Zhuang J, Wang Y, Ouellette ND, Turschak EE, Larsen RS, Takasaki KT, Daigle TL, Tasic B,
862 Waters J, Zeng H, Reid RC (2021) Laminar distribution and arbor density of two
863 functional classes of thalamic inputs to primary visual cortex. Cell Rep 37:109826.

864

865

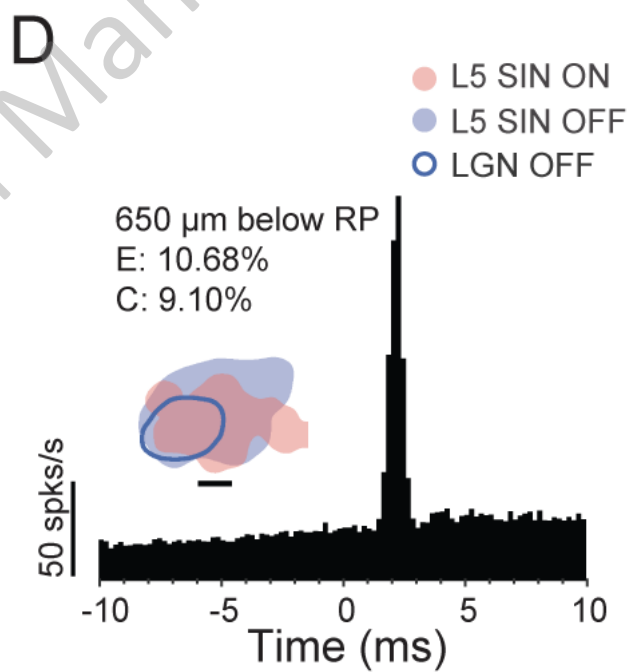
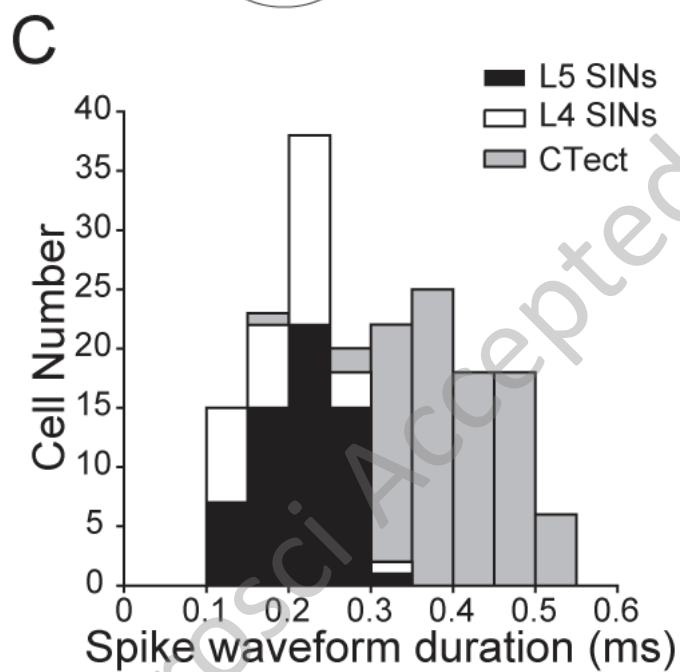
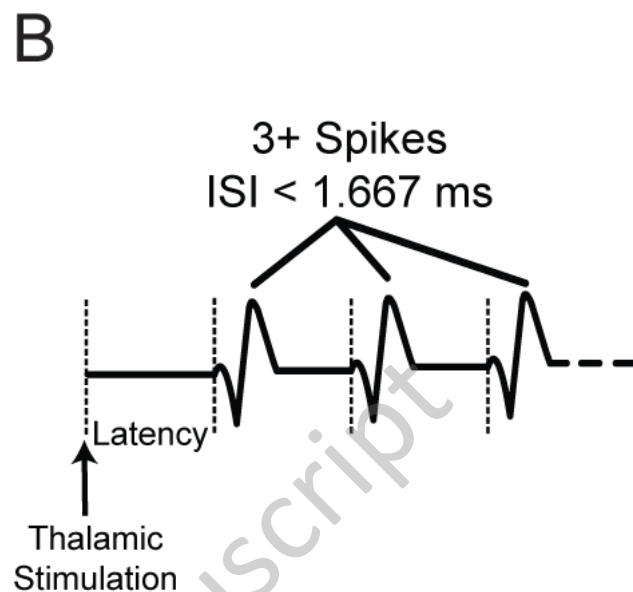
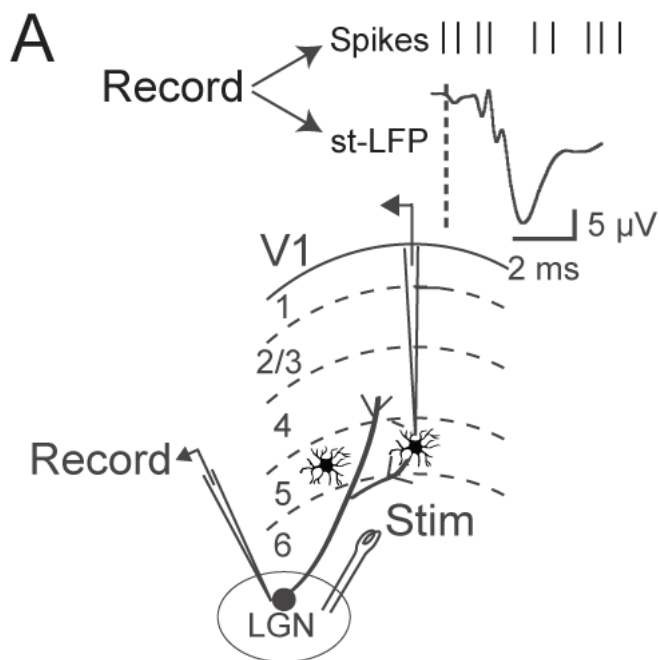
866 Table 1. Cell numbers of L5 SInS

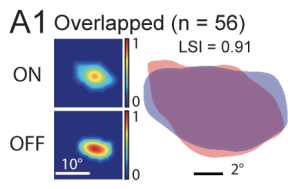
RF types	Number of cells	% of whole population
ON-OFF overlapped	56	86.15%
Single ON	4	6.15%
Single OFF	2	3.08%
Suppressive	2	3.08%
Not responding	1	1.54%
Total	65	100%

867

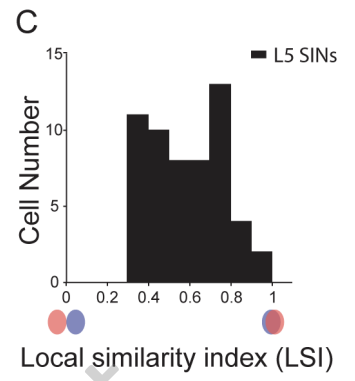
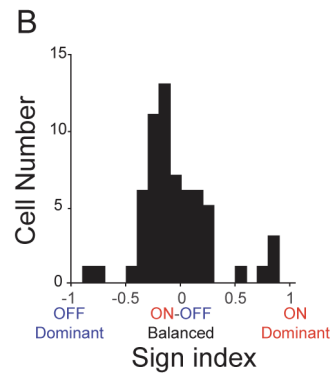
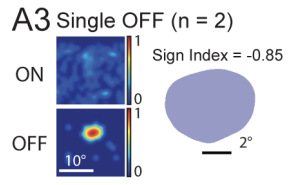
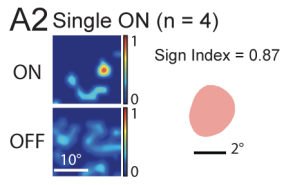
868

JNeurosci Accepted Manuscript

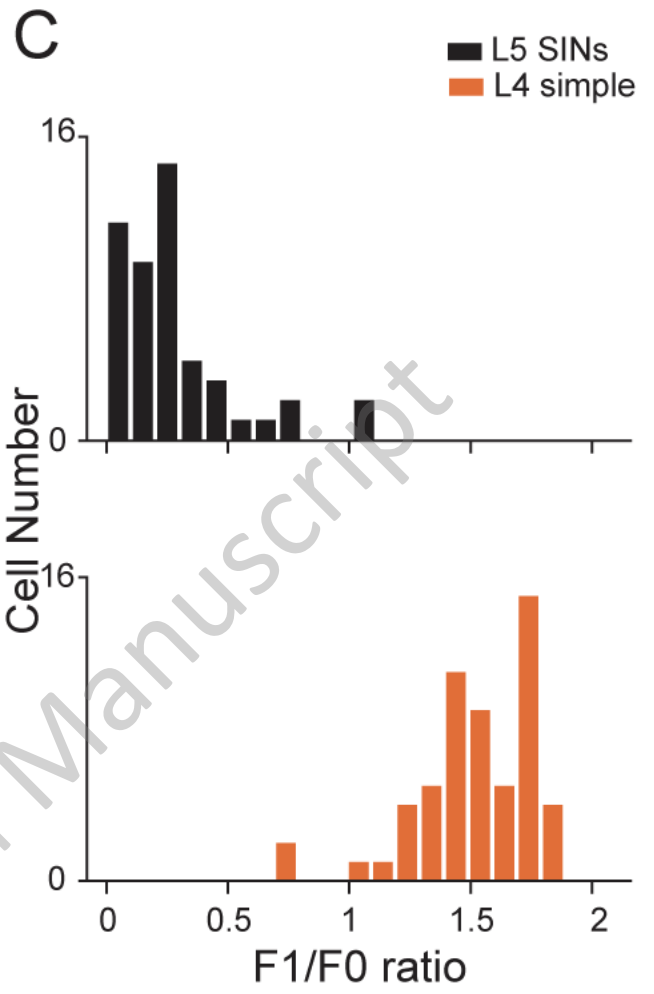
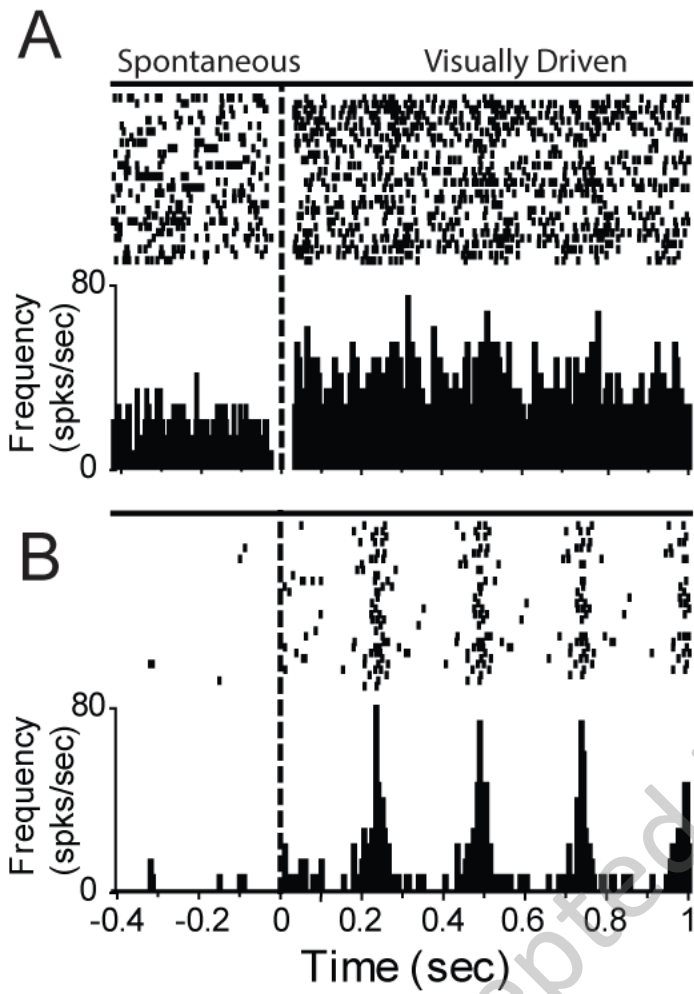


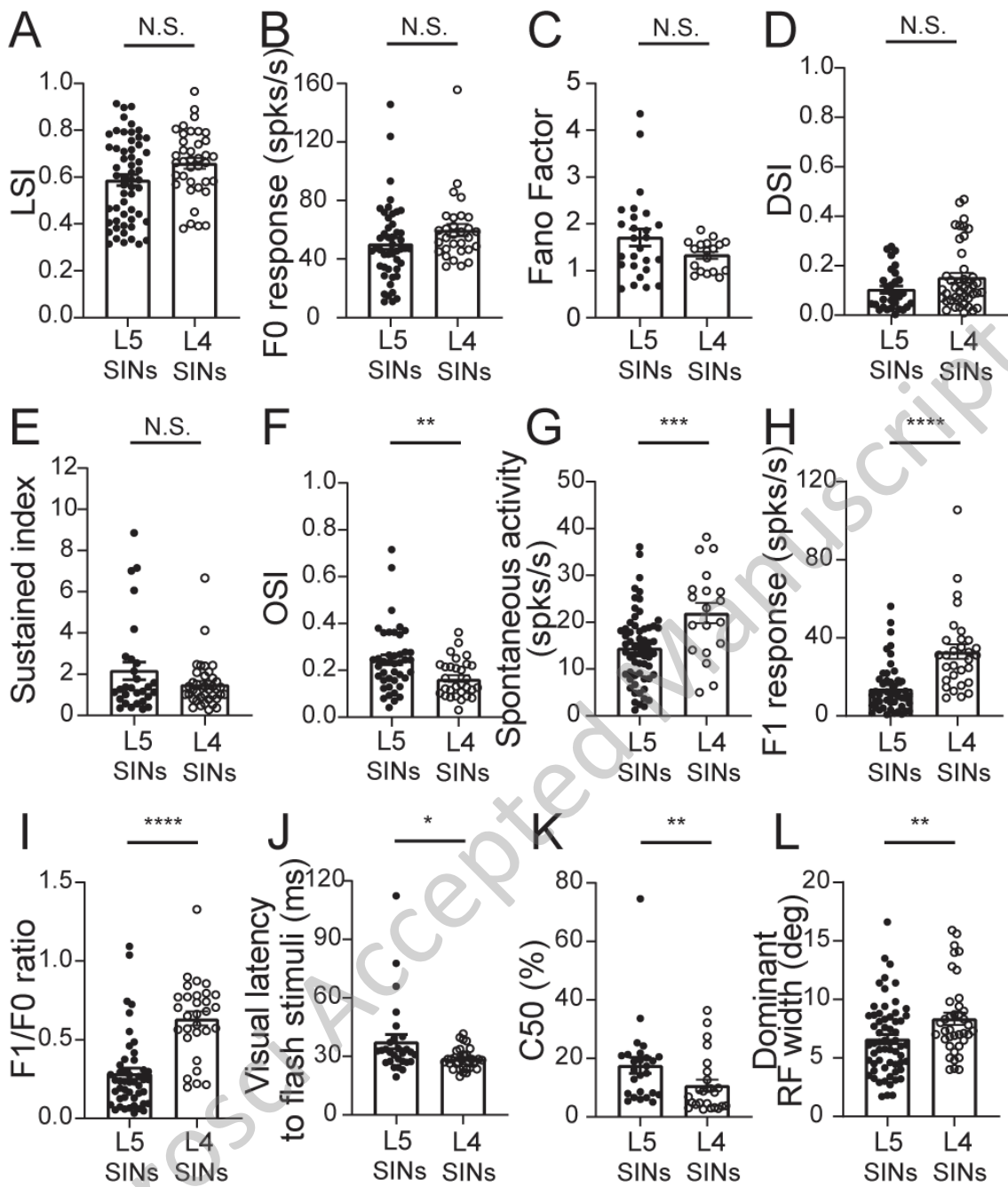


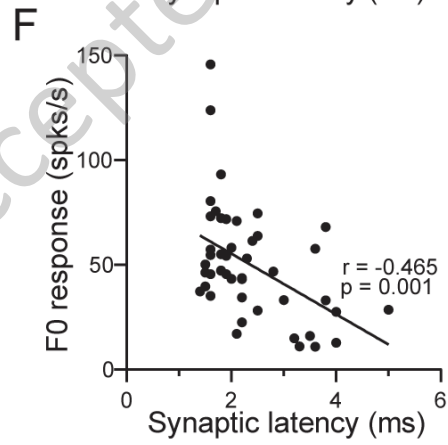
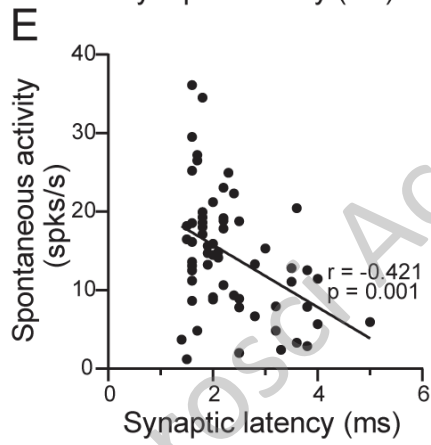
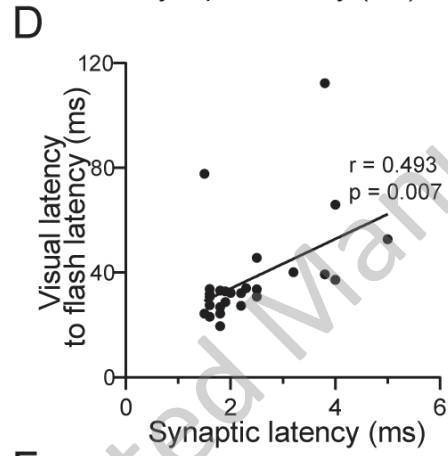
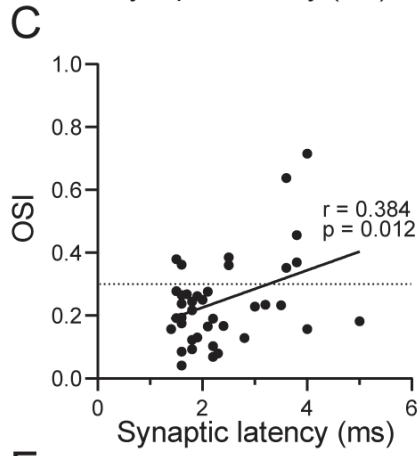
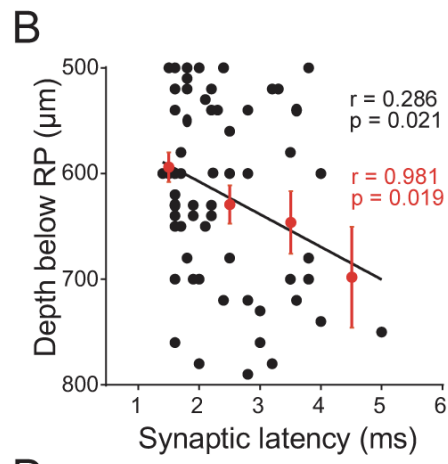
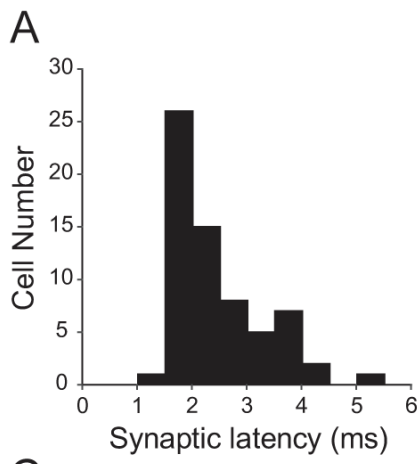
● ON
 ● OFF

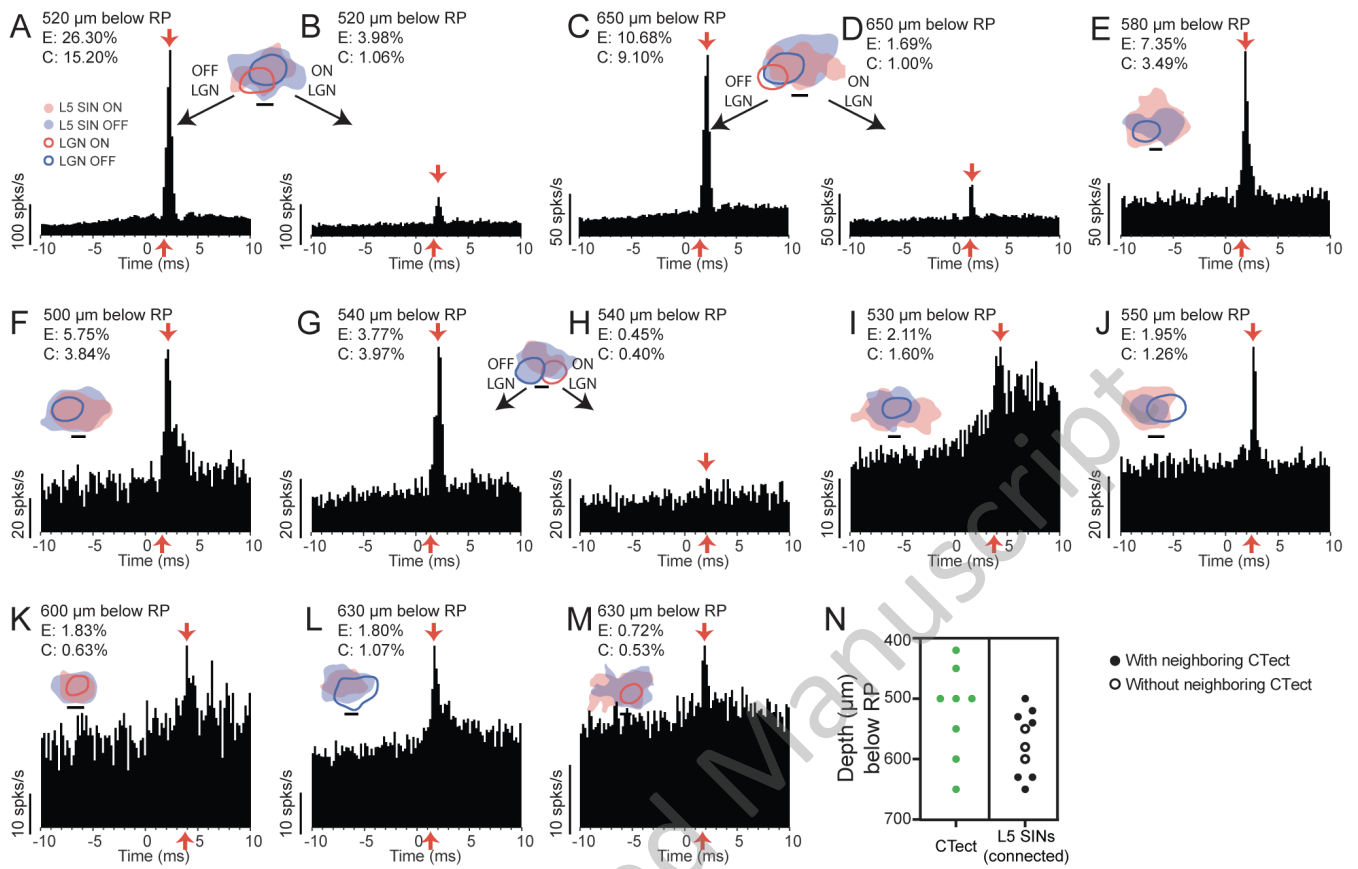


JNeurosci Accepted Manuscript

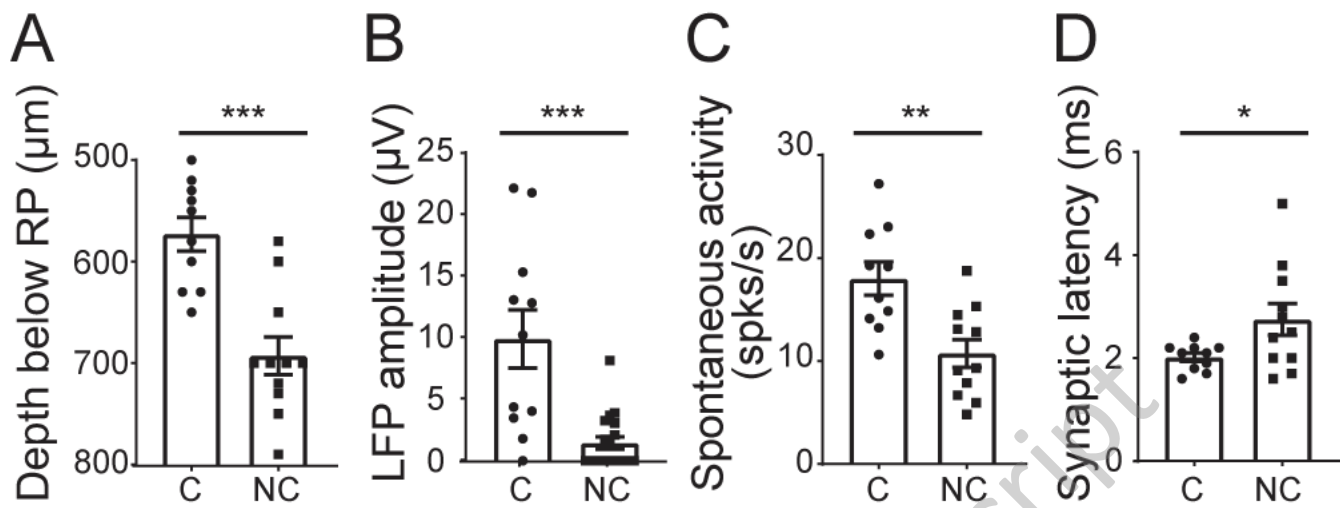








JNeurosci Accepted Manuscript



JNeurosci Accepted Manuscript